



# Compact TDLAS based optical sensor for ppb-level ethane detection by use of a 3.34 μm room-temperature CW interband cascade laser

Chunguang Li<sup>a,b</sup>, Lei Dong<sup>a,c,\*</sup>, Chuantao Zheng<sup>a,b</sup>, Frank K. Tittel<sup>a,\*\*</sup>

<sup>a</sup> Department of Electrical and Computer Engineering, Rice University, 6100 Main Street, Houston, TX 77005, USA

<sup>b</sup> State Key Laboratory on Integrated Optoelectronics, College of Electronic Science and Engineering, Jilin University, Changchun 130012, China

<sup>c</sup> State Key Laboratory of Quantum Optics and Quantum Optics Devices, Institute of Laser Spectroscopy, Shanxi University, Taiyuan 030006, China

## ARTICLE INFO

### Article history:

Received 8 February 2016

Received in revised form 25 March 2016

Accepted 25 March 2016

Available online 26 March 2016

### Keywords:

C<sub>2</sub>H<sub>6</sub> sensor

Infrared spectroscopy

Interband cascade laser

## ABSTRACT

A mid-infrared ethane (C<sub>2</sub>H<sub>6</sub>) sensor based on a wavelength modulation spectroscopy (WMS) technique was developed using a thermoelectrically cooled (TEC), continuous-wave (CW) interband cascade laser (ICL) emitting at 3.34 μm and a dense multi-pass gas cell (MPGC, 17 × 6.5 × 5.5 cm<sup>3</sup>) with a 54.6 m optical path length. A compact optical sensor system with a physical size of 35.5 × 18 × 12.5 cm<sup>3</sup> was designed and constructed. An ICL was employed for targeting a strong C<sub>2</sub>H<sub>6</sub> line at 2996.88 cm<sup>-1</sup> at <100 Torr gas pressure in the fundamental absorption band of C<sub>2</sub>H<sub>6</sub>. The sensor performance, including the minimum detection limit (MDL) and the stability were improved by reducing the effect of laser power drift by means of the 2f/1f-WMS technique. A MDL of ~1.2 parts per billion (ppbv) for 2f-WMS and ~1.0 ppbv for 2f/1f-WMS were achieved, respectively, with a measurement time of 4 s. The MDL was further improved from 299 pptv (@108 s for 2f-WMS) to 239 pptv (@208 s for 2f/1f-WMS), based on an Allan deviation analysis. The rise time (@0 → 100 ppbv) and fall time (@100 → 0 ppbv) were determined to be ~64 s and ~48 s, respectively, at a gas pressure of <100 Torr for the C<sub>2</sub>H<sub>6</sub> sensor operation.

© 2016 Elsevier B.V. All rights reserved.

## 1. Introduction

Ethane (C<sub>2</sub>H<sub>6</sub>) is the second-largest component of natural gas after methane (CH<sub>4</sub>) and is used in the chemical industry in the production of ethylene (C<sub>2</sub>H<sub>4</sub>) or as a feedstock in the manufacture of other commodity chemicals. C<sub>2</sub>H<sub>6</sub> is a combustible gas at room temperature and is explosive when it is mixed with 3–12.5% volume of air. C<sub>2</sub>H<sub>6</sub> occurs as a trace gas in the earth's atmosphere, at concentration levels of several ppbv, although its pre-industrial concentration levels were lower since a significant proportion of the ethane in the atmosphere originates from fossil fuels. Hence, as one of the most abundant non-methane hydrocarbons in the atmosphere at ppbv concentration level, C<sub>2</sub>H<sub>6</sub> influences both atmospheric chemistry and climate [1,2], and is therefore an important gas in environmental monitoring [3,4]. Furthermore, ultra-sensitive C<sub>2</sub>H<sub>6</sub> detection has also found

applications in human breath analysis as a non-invasive method to monitor and identify diseases, such as lung cancer, asthma, by the detection of C<sub>2</sub>H<sub>6</sub> concentrations in exhaled human breath [5–7].

Infrared tunable direct laser absorption spectroscopy (TDLAS) [8–10] enables non-contact trace gas measurements, and has proven to be an excellent tool for sensitive and selective detection in environmental [11–13], biomedical [14–20], industrial [21,22] and national security [13] applications. TDLAS requires a tunable laser exhibiting single frequency emission and a narrow linewidth at the targeted absorption line of a gas molecule in order to achieve high detection sensitivity and selectivity in the mid-infrared spectral range. Commercially available laser sources generally include semiconductor lasers, difference-frequency generation (DFG) [23], optical parametric oscillators (OPOs) [24] in the past, but in recent years quantum cascaded lasers (QCLs) [25] in the 3.7–12 μm spectral range and interband cascaded lasers (ICLs) in the 3–6 μm spectral range with low power-consumption [26] provide advantages in terms of continuous-wave (CW), distributed feedback (DFB) output power levels (up to hundreds of mW for QCLs and tens of mW for ICLs) and compactness. C<sub>2</sub>H<sub>6</sub> has strong absorption features in the 3–4 μm spectral region where its fundamental absorption band is located. C<sub>2</sub>H<sub>6</sub> detection with high precision and sensitivity takes advantage of a line strength of several orders of magnitude stronger than in the near infrared overtone absorption

\* Corresponding author at: State Key Laboratory of Quantum Optics and Quantum Optics Devices, Institute of Laser Spectroscopy, Shanxi University, Taiyuan 030006, China.

\*\* Corresponding author.

E-mail addresses: [donglei@sxu.edu.cn](mailto:donglei@sxu.edu.cn), [lei.dong@rice.edu](mailto:lei.dong@rice.edu) (L. Dong), [fkt@rice.edu](mailto:fkt@rice.edu) (F.K. Tittel).

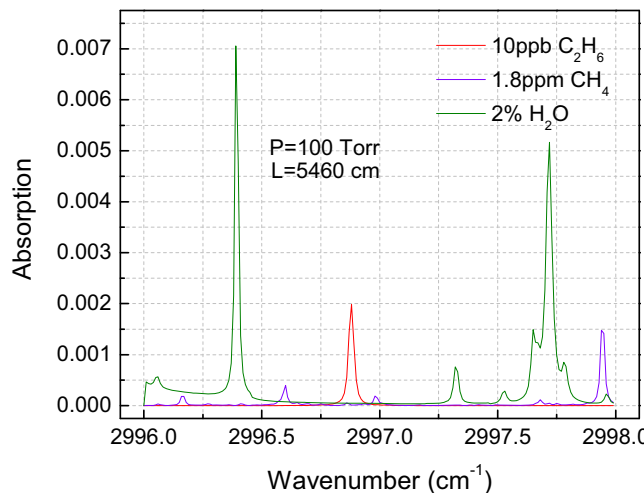


**Fig. 1.** HITRAN based absorption spectra of  $\text{C}_2\text{H}_6$  (10 ppbv),  $\text{CH}_4$  (1.8 ppmv), and  $\text{H}_2\text{O}$ (2%) in a narrow spectral range from  $2996\text{ cm}^{-1}$  to  $2998\text{ cm}^{-1}$  for a 5460 cm path length at a pressure of 100 Torr.  $\text{C}_2\text{H}_6$ ,  $\text{CH}_4$ , and  $\text{H}_2\text{O}$  lines are shown in red, purple, and green, respectively. (For interpretation of the references to colour in this figure legend, the reader is referred to the web version of this article.)

band. A mid-infrared  $\text{C}_2\text{H}_6$  absorption spectrometer using a TEC, DFB diode laser and a 57.6 m optical path-length multipass gas cell (MPGC) was reported in Ref. [27].  $\text{C}_2\text{H}_6$  measurements with a minimum detection limit (MDL) of 740 pptv were achieved at  $\sim 3.36\text{ }\mu\text{m}$  with a 1 s integration time. Furthermore  $\text{C}_2\text{H}_6$  measurements based on a CW, thermoelectrically cooled (TEC), DFB laser diode were performed with a 100 m optical path length astigmatic Herriott cell and a MDL of 240 pptv with a 1 s integration time was obtained [28]. Although these sensor systems achieved ppt detection sensitivities, they were too large to be suitable and convenient for some applications such as in field measurements (eg. mobile and airborne).

In this work, a compact  $\text{C}_2\text{H}_6$  sensor system based on a compact MPGC with a physical size of  $35.5 \times 18 \times 12.5\text{ cm}^3$  and a 54.6 m absorption length was employed. A TEC, CW, DFB, ICL centered at  $2996.88\text{ cm}^{-1}$  from Nanoplus (Germany) was used as the excitation source. The optical components were mounted on an aluminum plate, which provided good mechanical stability for sensing performance. Both 2f-wavelength modulation spectroscopy (WMS) and 2f/1f-WMS [29,30] techniques were adopted in the reported sensor system, and the latter technique was shown to be more stable for field applications.

## 2. Sensor configuration and optimization

### 2.1. Optimum $\text{C}_2\text{H}_6$ line selection

Most atmospheric trace gas species have strong fundamental absorption band in the mid-infrared spectral range, which facilitates the sensitive and selective detection of atmospheric trace gases in this spectral range. Ethane has a strong absorption band located at  $3.34\text{ }\mu\text{m}$ . At this wavelength, the potential spectral interferences mainly originate from methane ( $\text{CH}_4$ ) and water ( $\text{H}_2\text{O}$ ), which will affect the  $\text{C}_2\text{H}_6$  detection. High-resolution transmission molecular absorption database (HITRAN) is a worldwide standard for calculating or simulating atmospheric molecular transmission and radiation, which covers a wide spectral region from the microwave to the ultraviolet [31]. HITRAN absorption spectra of 10 ppb  $\text{C}_2\text{H}_6$ , 1.8 ppm  $\text{CH}_4$ , and 2%  $\text{H}_2\text{O}$  at a 100 Torr gas pressure and a 54.6-m effective optical path length are depicted in Fig. 1. A  $\text{C}_2\text{H}_6$  absorption line centered at  $3336.8\text{ nm}$  ( $2996.88\text{ cm}^{-1}$ ) was selected as the optimum  $\text{C}_2\text{H}_6$  target line. All the  $\text{H}_2\text{O}$  absorption lines (the two closest lines are located at  $2996.4\text{ cm}^{-1}$  and  $2997.3\text{ cm}^{-1}$ ) under an absolute humidity of 2% do not interfere with the selected  $\text{C}_2\text{H}_6$  line at  $2996.88\text{ cm}^{-1}$ , since they are  $\sim 0.5\text{ cm}^{-1}$  away. With a higher relative humidity, the dryers can be used to lower the  $\text{H}_2\text{O}$  concentration and thereby reduce the absolute humidity to an acceptable level, e.g. below 2%. In that case, the sensor can operate normally. Besides  $\text{H}_2\text{O}$  lines, a weak  $\text{CH}_4$  absorption line at  $2997\text{ cm}^{-1}$  is observed in the presence of 10 ppb  $\text{C}_2\text{H}_6$ , and the spacing between the two lines is  $\sim 0.12\text{ cm}^{-1}$  at a pressure of  $\sim 100$  Torr and a concentration of 1.8 ppm (i.e. the atmospheric concentration level). When the pressures is  $< 100$  Torr, the  $2997\text{ cm}^{-1}$   $\text{CH}_4$  line causes no interference to the  $\text{C}_2\text{H}_6$  line. However, the  $\text{C}_2\text{H}_6$  absorption line interferes once the pressure exceeds 150 Torr. Hence the pressure inside the MPGC must be  $< 150$  Torr in order to avoid overlapping of the  $\text{CH}_4$  and  $\text{C}_2\text{H}_6$  absorption lines.

### 2.2. Sensor design

The  $\text{C}_2\text{H}_6$  sensor architecture is depicted in Fig. 2(a), which includes both the optical and electrical sub-systems. In the optical part, a Nanoplus CW, DFB, TEC ICL was used as the excitation source and which is mounted in a TO66 header. The compact MPGC consists of two concave spherical mirrors capable of a novel, dense spot pattern, as shown in the insert of Fig. 2(b). Such a novel MPGC design offers a 54.6-m optical path length in a physical size of  $17 \times 6.5 \times 5.5\text{ cm}^3$  with a 220-mL sampling volume and results in a sensor platform that is more than 10 times smaller than conventional designs with equivalent sensitivity. In order to track the ICL beam, a dichroic mirror (ISP Optics, model BSP-

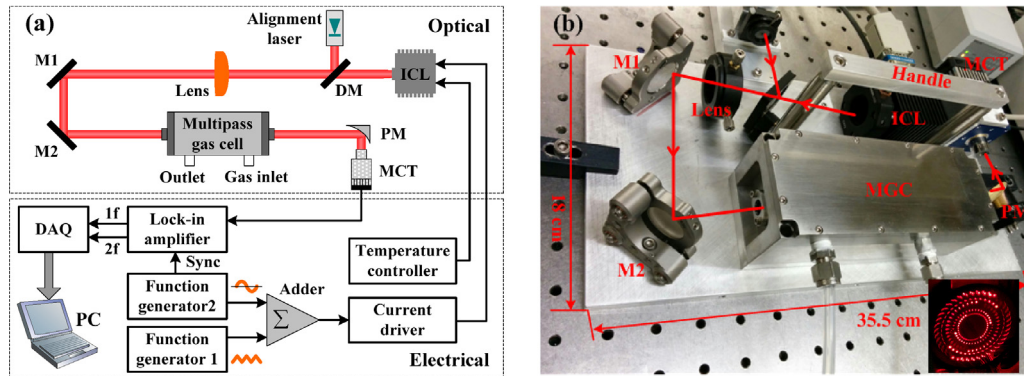


**Fig. 2.** (a) Schematic of the  $\text{C}_2\text{H}_6$  sensor based on a multipass gas cell and a  $3.337\text{ }\mu\text{m}$  CW, TEC ICL excitation source. ICL: interband cascade laser; DM: dichroic mirror; M: plane mirror; PM: parabolic mirror; MCT detector: mercury-cadmium-telluride detector; (b) Photo and physical dimensions of the compact sensor platform.

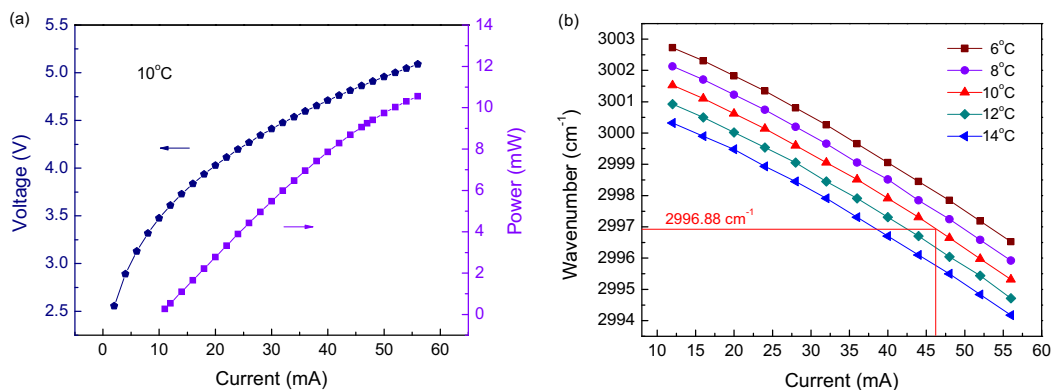


**Fig. 3.** Measured ICL output power and spectral tuning results for the 3.34  $\mu\text{m}$  CW TEC ICL at different operating temperatures and injection currents. (a) L-I-V curve for the laser operating at 10 °C. (b) Emission wavenumber plots for different ICL temperatures and driving currents.

DI-25-3) was used to combine a red alignment diode laser beam with the mid-infrared ICL beam. The combined laser beams were then coupled to the MPG using a mid-IR transmitting CaF<sub>2</sub> lens ( $d=25$  mm,  $f=200$  mm) and two adjustable plane mirrors (M1 and M2). The ICL beam enters the gas cell at the designed position and angle in order to achieve the 453 reflections of the ICL beam before exiting the MPG. The output beam is then focused onto a TEC mercury-cadmium-telluride (MCT) photodetector (VIGO System, model PVI-4TE-3.4) using a parabolic mirror (PM,  $d=25$  mm,  $f=35$  mm). The optical elements were mounted on an aluminum plate, as shown in the photo in Fig. 2(b).

The ICL current and temperature were controlled using a commercial current driver (Thorlabs, model LDC202C) and a temperature controller (Wavelength Electronics, model LFI-3751), respectively. Two electrical signals that included a triangular signal (0.3 Hz, 0.2 V<sub>pp</sub>) generated by a function generator 1 and a sinusoidal wave (5 kHz, optimized amplitude of 0.026 V, see Section 2.3) from function generator 2 were added and applied to the current driver to scan and modulate the ICL wavelength. A lock-in amplifier (LIA, Signal Recovery, model 7265) was used to demodulate the signal from the MCT detector by means of a synchronization signal from function generator 2, and both 1f and 2f harmonic signals were recorded at the LIA output. A data acquisition card (National Instrument, model USB-6356) was used to acquire the 1f and 2f spectra from the LIA for 2f-WMS and 2f/1f measurements. In addition, a compact, oil-free vacuum pump (Knf Neuberger Inc., model N 813.5 ANE/AF) and a pressure controller (MKS Instruments, Inc., Type 649) were used to pump gas into the MPG and to control the gas pressure inside the cell, respectively.

### 2.3. ICL characterization and optimization

The ICL has a wavelength of 3.337  $\mu\text{m}$  in order to target the C<sub>2</sub>H<sub>6</sub> absorption line at  $\sim 2996.88 \text{ cm}^{-1}$ . The Nanoplus TO66-mounted ICL (physical size: 5 × 5 × 5 cm<sup>3</sup>) can be operated at temperatures between 5 °C and 15 °C without forced air or water cooling. A Fourier transform infrared (FTIR) spectrometer (Thermo Scientific, model Nicolet 8700) and a power meter (Ophir Optoelectronics, model 3A) were employed to measure the ICL emission wavelength and power, respectively, at different driving currents. The measured I-V (current-voltage) and P-I (power-current) curves are shown in Fig. 3(a). The maximum measured optical power was  $\sim 10.5 \text{ mW}$  when the ICL was operated at a temperature of 10 °C and an injection current of 55 mA. The emission wavenumber can be tuned from 2994.2 cm<sup>-1</sup> to 3002.7 cm<sup>-1</sup>, as depicted in Fig. 3(b). The current and temperature wavelength-tuning coefficients for this ICL were experimentally determined to be  $-0.1415 \text{ cm}^{-1}/\text{mA}$  and  $-0.3014 \text{ cm}^{-1}/\text{°C}$ . An ICL injection current of 47 mA and a 10 °C

operating temperature were selected for C<sub>2</sub>H<sub>6</sub> concentration measurements at the interference-free absorption line of 2996.88 cm<sup>-1</sup>.

To optimize the sensor performance, both the gas pressure and the wavelength modulation depth (denoted by  $\Delta\nu$ ) must be appropriately chosen to achieve the highest 2f signal. For this purpose, a certified standard gas cylinder containing 1.14 ppm C<sub>2</sub>H<sub>6</sub> balanced by ultra-high purity (UHP) N<sub>2</sub> was employed for the optimization of the C<sub>2</sub>H<sub>6</sub> sensor system. Since the developed sensor will be primarily used for atmospheric C<sub>2</sub>H<sub>6</sub> detection, low-cost N<sub>2</sub> was chosen as the balance gas, which has a molecular weight similar to air. For each individual pressure ranging from 50 Torr to 200 Torr, the 2f signals were recorded with different modulation amplitudes, as depicted in Fig. 4. The modulation amplitude curve as a function of modulation depth is also plotted in Fig. 4. The results illustrate that the maximum C<sub>2</sub>H<sub>6</sub> 2f signal is achieved at a pressure of 200 Torr and a modulation depth of 0.142 cm<sup>-1</sup> which is based on the measured DC tuning coefficient. However, taking into account the interference from the CH<sub>4</sub> absorption line mentioned previously in Section 2.1 (see Fig. 1), the most suitable pressure and modulation depth are 100 Torr and 0.074 cm<sup>-1</sup>, respectively, corresponding to an amplitude of the modulation signal of  $\sim 0.026$  V. The selected absorption line width ( $\gamma$ ) is  $\sim 0.048 \text{ cm}^{-1}$  based on the HITRAN data base and an optimized modulation coefficient of  $\Delta\nu/\gamma = 1.58$  was achieved.

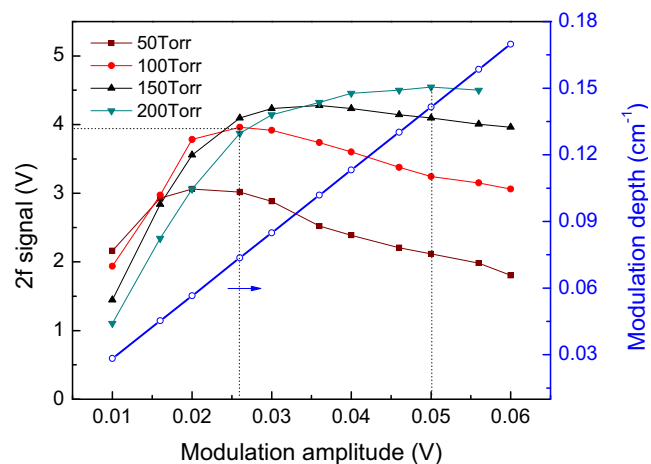


**Fig. 4.** Measured amplitude of the 2f signal and the modulation depth as a function of the modulation amplitude for a dry 200 ppb C<sub>2</sub>H<sub>6</sub>:N<sub>2</sub> mixture at four different pressure values.

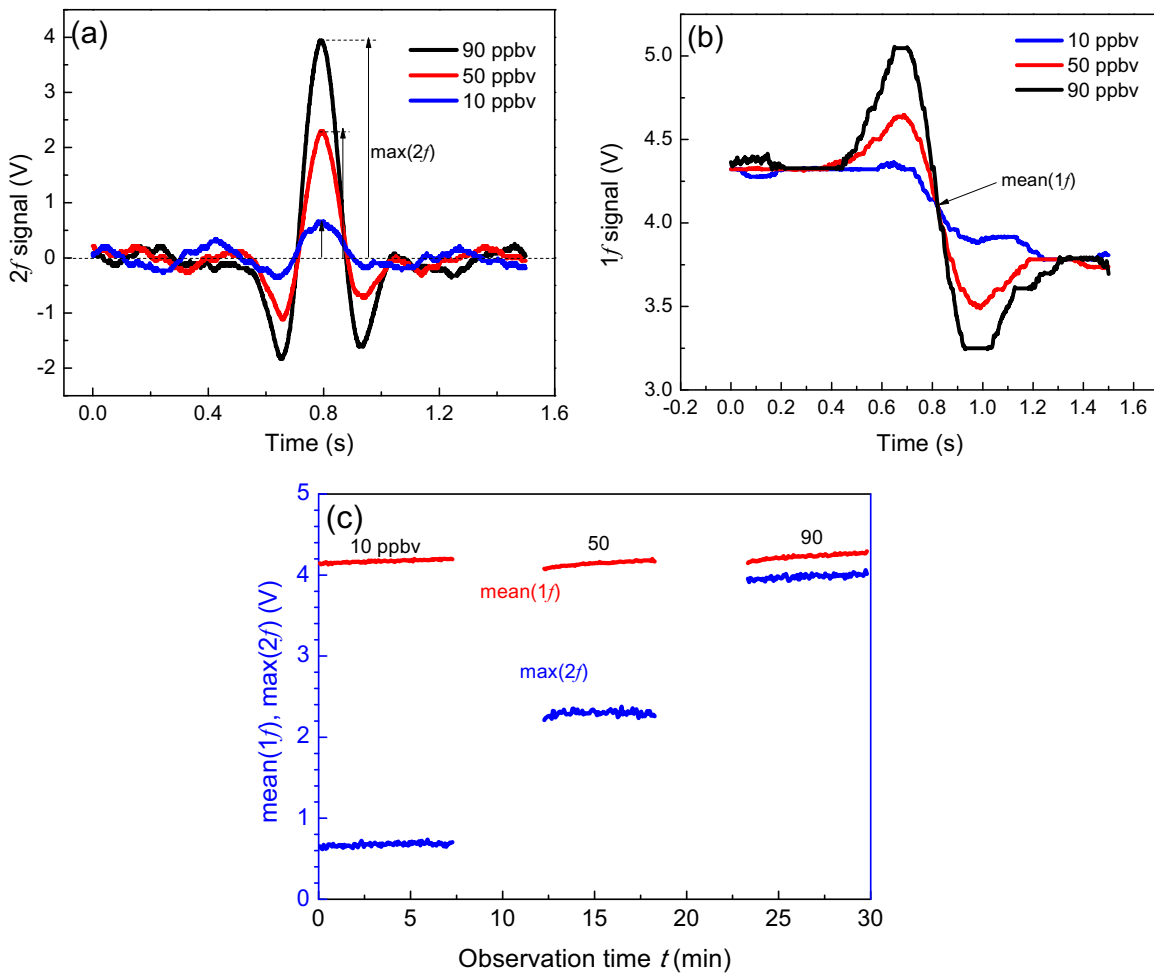


**Fig. 5.** Measured (a) 2f and (b) 1f waveforms for  $\text{C}_2\text{H}_6$  concentration levels of 90, 50, and 10 ppbv. (c) Max(2f) and mean(1f) plots versus observation time for concentrations of <90, 50, and 10 ppbv  $\text{C}_2\text{H}_6$ .

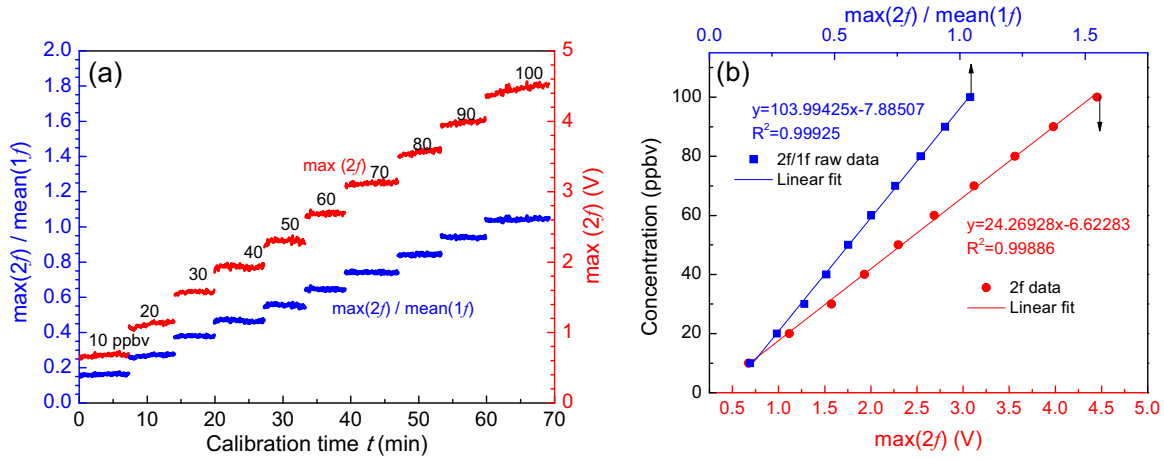


**Fig. 6.** (a) Measured curves of max(2f) and max(2f)/mean(1f) versus calibration time  $t$  for 10, 20, 30, 40, 50, 60, 70, 80, 90, 100 ppbv  $\text{C}_2\text{H}_6$  concentration levels. (b) Experimental dots and fitting curve of both max(2f) versus  $\text{C}_2\text{H}_6$  concentration and max(2f)/mean(1f) versus  $\text{C}_2\text{H}_6$  concentration levels.

### 3. Sensor performance assessment using 2f-WMS and 2f/1f-WMS modulation

#### 3.1. Experimental details

For both 2f-WMS and 2f/1f-WMS detection techniques, the driving current and laser temperature were set to 47 mA and 10 °C

for tuning the ICL wavelength to be centered at  $2996.88 \text{ cm}^{-1}$ . The pressure in the MPG was set to 100 Torr. The scan signal used a triangular signal with a frequency of 0.3 Hz and a peak-to-peak amplitude of 200 mV, and the modulation signal employed a sinusoidal signal with a frequency of 5 kHz and an amplitude of 0.026 V. The sensitivity of the lock-in amplifier was set to 50 mV, and the

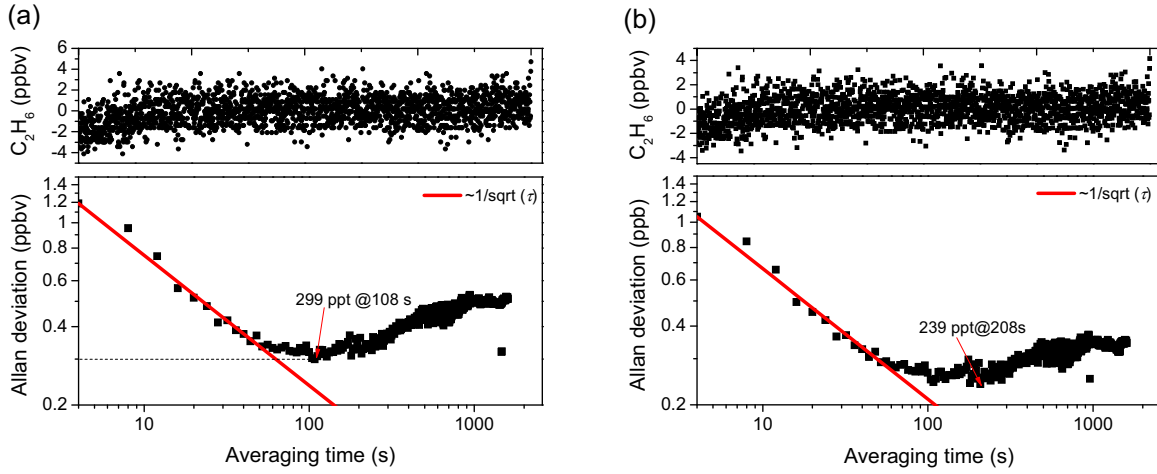


**Fig. 7.** Measured concentration for 0 ppbv  $C_2H_6$  concentration, versus time  $t$  and the Allan deviation as a function of integration time  $t$ , (a) 2f-WMS technique, (b) 2f/1f-WMS technique.

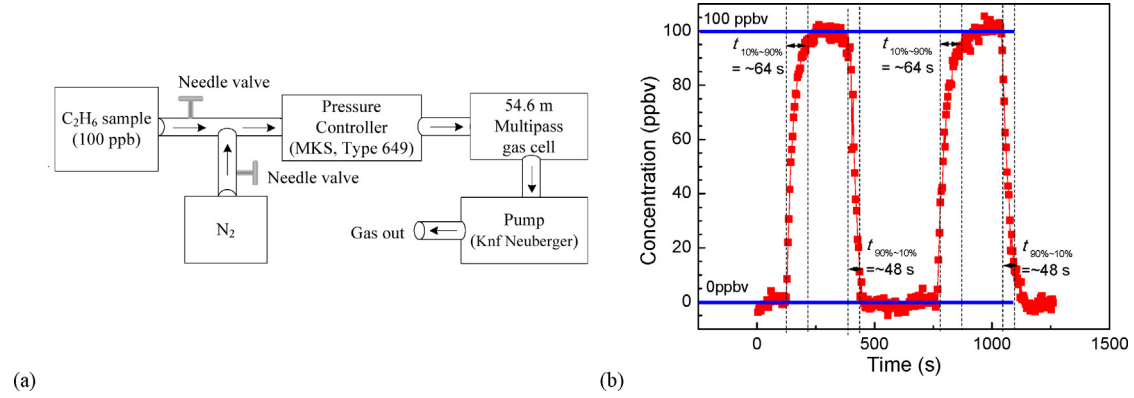


**Fig. 8.** (a) Schematic of a vacuum 'Y' feed line with two entrance ports and one exit port. (b) Response time measurement results by varying  $C_2H_6$  concentration levels between 0 and 100 ppbv.

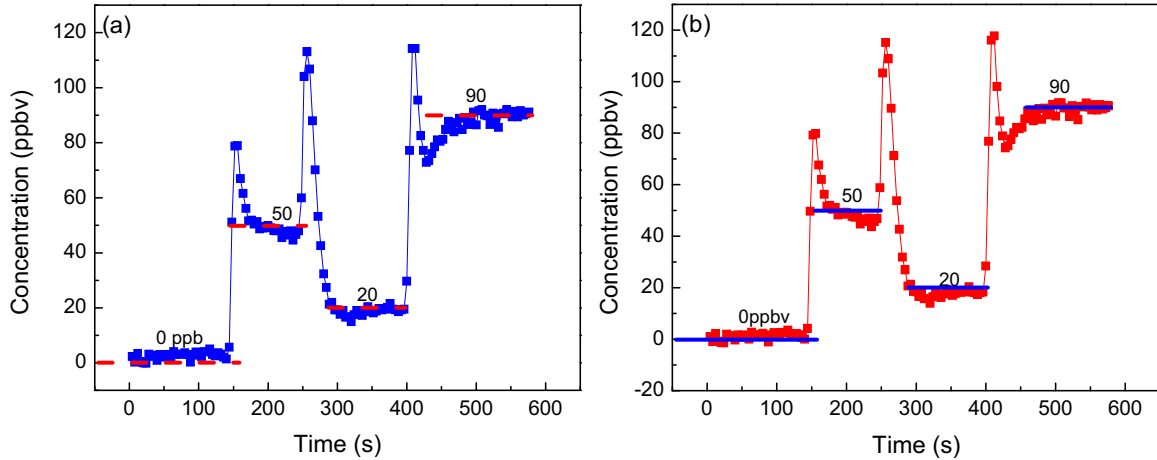


**Fig. 9.** Dynamic measurements of the  $C_2H_6$  sensor using (a) 2f-WMS technique and (b) 2f/1f-WMS technique, when  $C_2H_6$  concentration levels initially change from 0 ppbv to 50 ppbv, then decrease to 20 ppbv, and finally increase to 90 ppbv.

integration time to 10 ms. The generated 1f and 2f signals are sent to a DAQ card for data sampling. The sampling rate of the DAQ card was set to be 1 kHz, and as a result, each triangular period (including two  $C_2H_6$  spectra) contains 3333 data points. Data sampling was triggered by the triangular-wave scan signal to obtain the position of the peak value of the 2f signal during a scan (denoted by

$\max(2f)$ ), as depicted in Fig. 5(a)) as well as the position of the mean value of 1f signal (denoted by  $\text{mean}(1f)$ , as depicted in Fig. 5(b)). The  $\text{mean}(1f)$  value represents the average power of the laser, which can be used for minimizing the drift of the laser power and thus enhancing the sensor system stability [29]. Both the  $\max(2f)$  and  $\text{mean}(1f)$

data were recorded by the computer for subsequent processing and analysis.

$C_2H_6$  samples with different concentration levels (0–100 ppb) were prepared with a gas dilution system (Environics Inc., Series 4040). The 2f and 1f waveforms at concentration levels of 10, 50 and 90 ppb are shown in Fig. 5(a) and (b), respectively. In Fig. 5(a), the value of  $\text{max}(2f)$  increases as the concentration levels increase, due to the increased absorption at the peak absorption wavelength. In Fig. 5(b), the value of  $\text{mean}(1f)$  remains constant for the three selected concentrations. However, due to ICL power variations, both values will change for relatively long observation periods, as shown in Fig. 5(c). Furthermore, the three pairs of curves show the same variation trend. Hence, the ratio of  $\text{max}(2f)/\text{mean}(1f)$  can be used to reduce the effect of the ICL power drift.

### 3.2. Calibration and data-fitting

Ten  $C_2H_6$  samples covering a concentration range from 10 to 100 ppbv spaced 10 ppbv apart were prepared with the standard gas generator described in Section 3.1. The generated gas samples were pumped into the MPGC. Fig. 6(a) shows the measured value of  $\text{max}(2f)$  and the ratio of  $\text{max}(2f)/\text{mean}(1f)$  versus the calibration time  $t$ . Each sample was tested for ~7 min. The ratio of  $\text{max}(2f)/\text{mean}(1f)$  is more stable compared to  $\text{max}(2f)$  due to eliminating ICL power variations. The measured data of  $\text{max}(2f)$  and  $\text{max}(2f)/\text{mean}(1f)$  for each concentration were averaged and plotted as a function of the nominal concentration as shown in Fig. 6(b). A linear relation was observed between  $\text{max}(2f)$  and  $C$  and also between  $\text{max}(2f)/\text{mean}(1f)$  and  $C$  given by:

$$C = 24.26928\text{max}(2f) - 6.62283 \quad (1)$$

$$C = 103.99425\text{max}(2f)/\text{mean}(1f) - 7.88507 \quad (2)$$

In Eqs. (1) and (2), due to data-fitting errors, the intercepts of the two curves are not zero. Eqs. (1) and (2) with the measured data of  $\text{mean}(1f)$  and  $\text{max}(2f)$  will be used to determine the  $C_2H_6$  concentration levels.

### 3.3. Stability

Initially,  $C_2H_6$  measurements with zero gas were performed over a period of ~2 h, and the measured concentrations using both 2f-WMS and 2f/1f-WMS techniques were recorded. An Allan variance is utilized to analyze the stability and the minimum detection limit (MDL) for the two techniques. Fig. 7(a) exhibits the measured concentration versus time  $t$  and the Allan deviation as a function of the integration time  $t$  with the 2f-WMS technique. The plot indicates that the MDL is ~1.19 ppbv for a 4 s measurement time, and also shows an optimum integration time of 108 s corresponding to a MDL of ~299 pptv. The decreasing red solid line, which is proportional to  $(1/\tau)^{1/2}$ , indicates that the theoretical expected behavior of a system is dominated by white noise. For the 2f/1f-WMS technique, the Allan deviation as a function of integration time  $t$  is shown in Fig. 7(b). The MDL is ~1.05 ppbv for a 4 s measurement time. The Allan plot yields an optimum integration time of ~208 s with an MDL of 239 pptv, which is better than the MDL when using the 2f-WMS technique. Hence, the  $H_2C_6$  sensor system stability was improved by means of the 2f/1f-WMS technique.

### 3.4. Response time

A 'Y' feed line with two entrance ports and one exit port, as shown in Fig. 8(a) was implemented in order to determine the response time. The exit port was connected to the MPGC through a pressure controller. One entrance port was connected to the gas dilution system, through which the prepared gas sample was

supplied and the second entrance port was connected to the  $N_2$  cylinder. The two entrance ports could be switched "on" or "off" by two needle valves for the response time tests. With such a measurement scheme, the dynamic PID control process for the gas dilution system does not require to be considered, and the response time is determined by gas flow and cell volume. The measurement results are shown in Fig. 8(b) which indicate a 10–90% rise time and the 90–10% fall time of ~64 and ~48 s, respectively.

### 3.5. Dynamic measurements

The dynamic performance of the sensor was tested next. The output port of the gas dilution system was connected directly to the MPGC via the pressure controller. As shown in Fig. 9, the total measurement time was 600 s. The  $C_2H_6$  concentration initially changes from 0 ppbv to 50 ppbv, then decreases to 20 ppbv, and finally increases to 90 ppbv. The concentration level rises sharply, which implies that the sensor response time is shorter than the dynamic PID adjustment time. As the concentration increases, it takes more time for sample preparation and stabilizing the concentration levels. It was shown that the detection results of all samples were equal to the standard values, which illustrates an acceptable detection performance of the reported  $C_2H_6$  sensor system. Furthermore, there is no apparent difference between the 2f-WMS technique and 2f/1f-WMS technique because of the short observation time of each sample.

## 4. Conclusions

In this paper, we reported the design and performance of a mid-infrared  $C_2H_6$  sensor based on a compact optical platform and a CW, DFB, TEC ICL. A  $C_2H_6$  sensor system with a physical size of  $35.5 \times 18 \times 12.5 \text{ cm}^3$  was implemented, consisting of an ICL, a MCT detector, mirrors, and a MPGC with a physical size of  $17 \times 6.5 \times 5.5 \text{ cm}^3$ . The ICL with a wavelength of  $\sim 3.34 \mu\text{m}$  combined with 2f-WMS and 2f/1f-WMS was applied to an interference-free absorption line located at  $2996.88 \text{ cm}^{-1}$  at a pressure of 100 Torr in order to achieve  $C_2H_6$  measurements at ppb-level concentration levels. The optimum modulation depth was  $0.074 \text{ cm}^{-1}$ . The sensor performance was improved by reducing the effect of ICL power drift by means of the 2f/1f-WMS technique. The MDL is ~1.19 parts per billion (ppbv) for 2f-WMS and ~1.05 ppbv for 2f/1f-WMS techniques, respectively with a measurement time of 4 s. Furthermore, the sensor stability can be improved from 299 pptv (@108 s for the 2f-WMS method) to 239 pptv (@208 s using the 2f/1f-WMS method). The detection sensitivity and stability of the reported  $C_2H_6$  sensor system can be further improved by a redesign of the optical sensor components to further suppress optical fringes by implementing line-locking functionality which requires addition of a reference channel.

### Acknowledgments

Chunguang Li acknowledges support by China Scholarship Council (Grant No. 201406170107). Frank Tittel acknowledges support by the National Science Foundation (NSF) ERC MIRTHE award, a Robert Welch Foundation Grant C-0586, a NSF Phase II SBIR (Grant No. IIP-1230427) and by ARPA-E under award # DE AR0000547 and DE-AR0000545. Chuantao Zheng acknowledges the support by China Scholarship Council (Grant No. 201506175025), the National Natural Science Foundation of China (Grant No. 61307124), and the Changchun Municipal Science and Technology Bureau (Grant No. 14KG022). Lei Dong acknowledges support by National Natural Science Foundation of China (Grant Nos. 61575113 and 61275213).

## References

- [1] I.J. Simpson, F.S. Rowland, S. Meinardi, D.R. Blake, Influence of biomass burning during recent fluctuations in the slow growth of global tropospheric methane, *Geophys. Res. Lett.* 33 (2006) L22808.
- [2] Y. Xiao, J.A. Logan, D.J. Jacob, R.C. Hudman, R. Yantosca, D.R. Blake, Global budget of ethane and regional constraints on U.S. sources, *J. Geophys. Res.* 113 (2008) D21306.
- [3] L.C. Thomson, B. Hirst, G. Gibson, S. Gillespie, P. Jonathan, K.D. Skeldon, M.J. Padgett, An improved algorithm for locating a gas source using inverse methods, *Atmos. Environ.* 41 (2007) 1128–1134.
- [4] G. Etiopic, P. Ciccioli, Earth's degassing: a missing ethane and propane source, *Science* 323 (5913) (2009) 478.
- [5] P. Paredi, S.A. Kharitonov, P.J. Barnes, Elevation of exhaled ethane concentration in asthma, *Am. J. Respir. Crit. Care Med.* 162 (2000) 1450–1454.
- [6] B.K. Puri, B.M. Ross, I.H. Treasaden, Increased levels of ethane a non-invasive, quantitative, direct marker of n-3 lipid peroxidation, in the breath of patients with schizophrenia, *Prog. Neuropsychopharmacol. Biol. Psychiatry* 32 (2008) 858–862.
- [7] K.D. Skeldon, L.C. McMillan, C.A. Wyse, S.D. Monk, G. Gibson, C. Patterson, T. France, C. Longbottom, M.J. Padgett, Application of laser spectroscopy for measurement of exhaled ethane in patients with lung cancer, *Respir. Med.* 100 (2006) 300–306.
- [8] J.A. Silver, Frequency-modulation spectroscopy for trace species detection: theory and comparison among experimental methods, *Appl. Opt.* 31 (6) (1992) 707–717.
- [9] P. Werle, A review of recent advances in semiconductor laser based gas monitors, *Spectrochim. Acta A* 54 (1998) 197–236.
- [10] S. Schilt, L. Thévenaz, P. Robert, Wavelength modulation spectroscopy: combined frequency and intensity laser modulation, *Appl. Opt.* 42 (33) (2003) 6728–6738.
- [11] G. Wysocki, Y. Bakirkin, S. So, F.K. Tittel, C.J. Hill, R.Q. Yang, M.P. Fraser, Dual interband cascade laser based trace-gas sensor for environmental monitoring, *Appl. Opt.* 46 (33) (2007) 8202–8210.
- [12] M.N. Fiddler, I. Begashaw, M.A. Mickens, M.S. Collingwood, Z. Assefa, S. Bililign, Laser spectroscopy for atmospheric and environmental sensing, *Sensors* 9 (2009) 10447–10512.
- [13] R.F. Curl, F. Capasso, C. Gmachl, A.A. Kosterev, B. McManus, R. Lewicki, M. Pusharsky, G. Wysocki, F.K. Tittel, Quantum cascade lasers in chemical physics, *Chem. Phys. Lett. Front. Artic.* 487 (2010) 1–18.
- [14] M.R. McCurdy, Y. Bakirkin, G. Wysocki, R. Lewicki, F.K. Tittel, Recent advances of laser –spectroscopy-based techniques for applications in breath analysis, *J. Breath Res.* 1 (2007) 014001.
- [15] T.H. Risby, F.K. Tittel, Current status of midinfrared quantum and interband cascade lasers for clinical breath analysis, *SPIE Opt. Eng.* 49 (11) (2010) 111123.
- [16] J.H. Shorter, D.D. Nelson, J.B. McManus, M.S. Zahniser, D.K. Milton, Multicomponent breath analysis with infrared absorption using room-temperature quantum cascade lasers, *IEEE Sens. J.* 10 (1) (2010) 76–84.
- [17] J.H. Shorter, D.D. Nelson, J.B. McManus, M.S. Zahniser, S.R. Sama, D.K. Milton, Clinical study of multiple breath biomarkers of asthma and COPD (NO CO<sub>2</sub>, CO and N<sub>2</sub>O) by infrared laser spectroscopy, *J. Breath Res.* 5 (2011) 037108.
- [18] M.R. McCurdy, A. Sharafkhaneh, H. Abdel-Monem, J. Rojo, F.K. Tittel, Exhaled nitric oxide parameters and functional capacity in chronic obstructive pulmonary disease, *J. Breath Res.* 5 (2011) 016003.
- [19] K.R. Parameswaran, D.I. Rosen, M.G. Allan, A.M. Ganz, T.H. Risby, Off-axis integrated cavity output spectroscopy with a mid-infrared interband cascade laser for real-time breath ethane measurements, *Appl. Opt.* 48 (4) (2009) B73–B79.
- [20] D. Halmer, S. Thelen, P. Hering, M. Murtz, Online monitoring of ethane traces in exhaled breath with a difference frequency generation spectrometer, *Appl. Phys. B* 85 (2006) 437–443.
- [21] G. Wysocki, A.A. Kosterev, F.K. Tittel, Spectroscopic trace-gas sensor with rapidly scanned wavelengths of a pulsed quantum cascade laser for in situ NO monitoring of industrial exhaust systems, *Appl. Phys. B* 80 (2005) 617–625.
- [22] M. Lewander, Z.G. Guan, L. Persson, A. Olson, S. Svanberg, Food monitoring based on diode laser gas spectroscopy, *Appl. Phys. B* 93 (2008) 619–625.
- [23] J. Chen, S. So, H. Lee, M.P. Fraser, R.F. Curl, T. Harman, F.K. Tittel, Atmospheric formaldehyde monitoring in the Greater Houston area in 2002, *Appl. Spectrosc.* 58 (2) (2004) 243–247.
- [24] M. Angelmahr, A. Miklos, P. Hess, Photoacoustic spectroscopy of formaldehyde with tunable laser radiation at the parts per billion level, *Appl. Phys. B* 85 (2–3) (2006) 285–288.
- [25] J. Li, U. Parchatka, H. Fischer, A formaldehyde trace gas sensor based on a thermoelectrically cooled CW-DFB quantum cascade laser, *Anal. Methods* 6 (15) (2014) 5483–5488.
- [26] J.H. Miller, Y.A. Bakirkin, T. Ajtai, F.K. Tittel, C.J. Hill, R.Q. Yang, Detection of formaldehyde using off-axis integrated cavity output spectroscopy with an interband cascade laser, *Appl. Phys. B* 85 (2–3) (2006) 391–396.
- [27] K. Krzempek, M. Jahjah, R. Lewicki, P. Stefanski, S. So, D. Thomazy, F.K. Tittel, CW DFB RT diode laser-based sensor for trace-gas detection of ethane using a novel compact multipass gas absorption cell, *Appl. Phys. B* 112 (2013) 461–465.
- [28] K. Krzempek, R. Lewicki, L. Naehle, M. Fischer, J. Koeth, S. Belahsene, Y. Rouillard, L. Worschech, F.K. Tittel, Continuous wave, distributed feedback diode laser based sensor for trace-gas detection of ethane, *Appl. Phys. B* 106 (2012) 251–255.
- [29] G.B. Rieker, J.B. Jeffries, R.K. Hanson, Calibration-free wavelength-modulation spectroscopy for measurements of gas temperature and concentration in harsh environments, *Appl. Opt.* 48 (29) (2009) 5546–5560.
- [30] L.J. Lan, Y.J. Ding, Z.M. Peng, Y.J. Du, Y.F. Liu, Calibration-free wavelength modulation for gas sensing in tunable diode laser absorption spectroscopy, *Appl. Phys. B* 117 (2014) 1211–1219.
- [31] L.S. Rothman, I.E. Gordon, Y. Babikov, A. Barbe, D. Chris Benner, P.F. Bernath, M. Birk, L. Bizzocchi, V. Boudon, L.R. Brown, A. Campargue, K. Chance, E.A. Cohen, L.H. Couder, V.M. Devi, B.J. Drouin, A. Fayt, J.-M. Flaud, R.R. Gamache, J.J. Harrison, J.-M. Hartmann, C. Hill, J.T. Hodges, D. Jacquemart, A. Jolly, J. Lamouroux, R.J. LeRoy, G. Li, D.A. Long, O. Lyulin, C. Mackie, S.T. Massie, S. Mikhailenko, H.S. Müller, O. Naumenko, A. Nikitin, J. Orphal, V.I. Perevalov, A. Perrin, E.R. Polovtseva, C. Richard, M.A.H. Smith, E. Starikova, K. Sung, S. Tashkun, J. Tennyson, G.C. Toon, VI G. Tyuterev, G. Wagner, The HITRAN 2012 molecular spectroscopic database, *J. Quant. Spectrosc. Radiat. Transfer* 130 (2013) 4–50.

## Biographies

**Chunguang Li** received his B.S. degree in communications engineering from Changchun University of Science and Technology, PR China, in 2009. He is now pursuing a Ph.D. degree in circuits and systems from the College of Electronic Science and Engineering at Jilin University. His research interests include gas sensors, circuit design and control, and laser spectroscopy.

**Lei Dong** received his Ph.D. degree in optics from Shanxi University, China, in 2007. From June, 2008 to December, 2011, he worked as a post-doctoral fellow in the Electrical and Computer Engineering Department and Rice Quantum Institute, Rice University, Houston, USA. Currently he is a professor in the Institute of Laser Spectroscopy of Shanxi University. His research interests include optical sensors, trace gas detection, and laser spectroscopy.

**Chuantao Zheng** received his MS degree and Ph.D degree in 2007 and 2010, respectively, from the College of Electronic Science and Engineering, Jilin University, PR China. Now he is an associate professor in the same college. His research interests include optoelectronic devices and its applications in gas sensing and optical communications.

**Frank K. Tittel** received his B.S. degree in 1955 and the Ph.D. degree in 1959 from Oxford University. Now he is the J. S. Abercrombie Professor in the School of Engineering, Rice University, Houston, USA. Professor Frank Tittel has been involved in many innovative developments in quantum electronics and laser technology since the discovery of the laser in 1960, with applications ranging from laser spectroscopy to environmental monitoring. The most recent designs utilize novel quantum cascade and interband cascade lasers to achieve compact, robust instrumentation that can be deployed for field applications, such as at NASA's Johnson Space Center related to air and water quality issues relevant to the International Space Station, for urban formaldehyde monitoring funded by the Environmental Protection Agency, and by the National Institute of Health, for non-invasive NO and CO detection in biomedical systems by the National Institute of Health and the National Science Foundation (<http://lasersci.rice.edu/>).